



**HAL**  
open science

# Original Application of Stop-Band Negative Group Delay Microwave Passive Circuit for Two-Step Stair Phase Shifter Designing

Blaise Ravelo, Glauco Fontgalland, Hugerles Silva, Jamel Nebhen, Wenceslas Rahajandraibe, Mathieu Guerin, George Chan, Fayu Wan

► **To cite this version:**

Blaise Ravelo, Glauco Fontgalland, Hugerles Silva, Jamel Nebhen, Wenceslas Rahajandraibe, et al.. Original Application of Stop-Band Negative Group Delay Microwave Passive Circuit for Two-Step Stair Phase Shifter Designing. IEEE Access, 2021, 10 (1493-1508), 10.1109/ACCESS.2021.3138371 . hal-03509428

**HAL Id: hal-03509428**

**<https://hal.science/hal-03509428>**

Submitted on 7 Mar 2023

**HAL** is a multi-disciplinary open access archive for the deposit and dissemination of scientific research documents, whether they are published or not. The documents may come from teaching and research institutions in France or abroad, or from public or private research centers.

L'archive ouverte pluridisciplinaire **HAL**, est destinée au dépôt et à la diffusion de documents scientifiques de niveau recherche, publiés ou non, émanant des établissements d'enseignement et de recherche français ou étrangers, des laboratoires publics ou privés.

## AUTHOR QUERIES

### AUTHOR PLEASE ANSWER ALL QUERIES

PLEASE NOTE: Please note that we cannot accept new source files as corrections for your article. If possible, please annotate the PDF proof we have sent you with your corrections and upload it via the Author Gateway. Alternatively, you may send us your corrections in list format. You may also upload revised graphics via the Author Gateway.

Carefully check the page proofs (and coordinate with all authors); additional changes or updates WILL NOT be accepted after the article is published online/print in its final form. Please check author names and affiliations, funding, as well as the overall article for any errors prior to sending in your author proof corrections. Your article has been peer reviewed, accepted as final, and sent in to IEEE. No text changes have been made to the main part of the article as dictated by the editorial level of service for your publication.

- AQ:1 = Please confirm or add details for any funding or financial support for the research of this article.
- AQ:2 = Please provide the expansion of the acronym NUIST for your funding agency. Providing the correct acknowledgement will ensure proper credit to the funder.
- AQ:3 = If you haven't done so already, please make sure you have submitted a graphical abstract for your paper. The GA should be a current figure or image from your accepted article. The GA will be displayed on your articles abstract page on IEEE Xplore. Please choose a current figure from the paper and supply a caption at your earliest convenience for the graphical abstract. Note that captions cannot exceed 1800 characters (including spaces). If you submitted a video as your graphical abstract, please make sure there is an overlay image and caption. Overlay images are usually a screenshot of your video that best represents the video. This is for readers who may not have access to video-viewing software. Please see an example in the link below: <http://ieeaccess.ieee.org/submitting-an-article/>
- AQ:4 = Please provide the date for Ref. [18].
- AQ:5 = Please provide the volume no. and issue no. or month for Ref. [38].
- AQ:6 = Please provide a better/higher quality images for the authors Glauco Fontgalland and Fayu Wan.
- AQ:7 = Please provide the year of completion when the author Mathieu Guerin received the Ph.D. degree.

Received November 20, 2021, accepted December 22, 2021. Date of publication xxxx 00, 0000, date of current version xxxx 00, 0000.

Digital Object Identifier 10.1109/ACCESS.2021.3138371

# Original Application of Stop-Band Negative Group Delay Microwave Passive Circuit for Two-Step Stair Phase Shifter Designing

**BLAISE RAVELO<sup>1</sup>**, (Member, IEEE), **GLAUCO FONTGALLAND<sup>2</sup>**, (Senior Member, IEEE), **HUGERLES S. SILVA<sup>3</sup>**, (Member, IEEE), **JAMEL NEBHEN<sup>4</sup>**, (Member, IEEE), **WENCESLAS RAHAJANDRAIBE<sup>5</sup>**, (Member, IEEE), **MATHIEU GUERIN<sup>5</sup>**, (Member, IEEE), **GEORGE CHAN<sup>6</sup>**, (Senior Member, IEEE), **AND FAYU WAN<sup>1</sup>**, (Member, IEEE)

<sup>1</sup>School of Electronic and Information Engineering, Nanjing University of Information Science & Technology, Nanjing 210044, China

<sup>2</sup>Applied Electromagnetic and Microwave Laboratory, Federal University of Campina Grande, Campina Grande 58429-830, Brazil

<sup>3</sup>Instituto de Telecomunicações, Universidade de Aveiro, Campus Universitário de Santiago, 3810-193 Aveiro, Portugal

<sup>4</sup>College of Computer Engineering and Sciences, Prince Sattam Bin Abdulaziz University, Al-Kharj 11942, Saudi Arabia

<sup>5</sup>Aix-Marseille University, CNRS, University of Toulon, IM2NP UMR7334, 13397 Marseille, France

<sup>6</sup>ASM Pacific Technology Ltd., Hong Kong

Corresponding author: Jamel Nebhen (j.nebhen@psau.edu.sa)

AQ:1  
AQ:2

This work was supported in part by the National Natural Science Foundation of China (NSFC) under Grant 61971230, in part by the Jiangsu Specially Appointed Professor Program and Six Major Talents Summit of Jiangsu Province under Grant 2019-DZXX-022, in part by the Startup Foundation for Introducing Talent of NUIST, and in part by the Deanship of Scientific Research at Prince Sattam Bin Abdulaziz University, Saudi Arabia.

AQ:3

**ABSTRACT** This paper investigates on the theorization, design, fabrication and measurement of original phase shifter (PS) operating with two-step stair phase behavior. The innovative stair PS is designed with unfamiliar stop-band (SB) negative group delay (NGD) passive circuit. The elementary unfamiliar SB-NGD topology constituted by resistive, inductive, and capacitive lumped network is described. Acting as an RF and microwave circuit, the S-matrix model is expressed in function the RLC-network parameters. Thus, the canonical form of unfamiliar SB-NGD transfer function (TF) represented by the transmission coefficient is established. The unfamiliar SB-NGD circuit equations in terms of the NGD parameters are formulated. The established theory is validated comparing the calculated, simulated, and measured S-parameters and group delays (GDs). Results with a very good agreement showing unfamiliar SB-NGD behavior are observed around the central frequency 2.45 GHz and bandwidth of 100 MHz. An innovative application of unfamiliar SB-NGD function for the communication system front-end is developed. The developed application concept of unfamiliar SB-NGD circuit is illustrated by designing a microwave device operating as a PS presenting a two-step stair response completely original behavior. The basic theory, design and implementation of the two-step stair PS concept are introduced. To validate the two-step stair PS principle, a proof of concept (PoC) is designed based distributed element based inductive and capacitive microstrip elements. The simulated and measured results of the PS PoC are in good agreement. The experimental results confirm the feasibility of two-step stair PS with phase jumping from  $-70^\circ \pm 4^\circ$  (from 2 GHz to 2.3 GHz) to  $-104^\circ \pm 2^\circ$  (from 2.6 GHz to 3.0 GHz). The investigated unfamiliar SB-NGD function-based stair PS is promising for future development 5G and 6G communication system.

**INDEX TERMS** Circuit theory, innovative concept, design method, microwave circuit, passive topology, S-parameter model, stop-band (SB) negative group delay (NGD), SB-NGD application, stair phase shifter (PS).

## I. INTRODUCTION

The massive deployment of 5G technology constitutes a bridging step of future wireless communication. To meet

The associate editor coordinating the review of this manuscript and approving it for publication was Venkata Rajesh Pamula.

the expected users demand, innovative design of front-end RF and microwave circuit ensuring accurate performance of radiation pattern is necessary [1]. This radiation performance is essentially ensured with improvement of beam-steering antenna array design [2]–[4]. Different antenna array topologies as adaptive [2] and coupled phased looped

array [3] have been proposed. But these topologies need to be improved to suppress the RF impairment in massive antenna arrays [4]. To increase the compactness and linearity, an innovative topology of metamaterial-based array antenna was proposed [5], [6]. Such antenna arrays operate with linear metamaterial-based phase shifters [7].

The elaboration of negative refractive index (NRI) aspect of metamaterial was an inspiration for the emerging RF and microwave function operating with bandpass (BP) negative group delay (NGD) [8], [9]. The NRI structures are also known to operate with negative group velocity (NGV) effect. The metamaterial BP-NGD circuits were implemented with significantly lossy periodical cells [8], [9]. Therefore, RF and microwave engineers wondered curiously on the existence of BP-NGD circuit application. To answer, tentative applications were suggested [10]–[24]. The BP-NGD function was introduced for adaptative aspect in a microwave signal processing building block [10]. Then, the NGD circuit was also proposed for the compensation of microwave devices [11].

However, the natural NGD application is the group delay (GD) equalization [12]–[14], which was proposed for the microwave signal RC-network based interconnects [12], [13] and also the BP filter GD rabbit ear reduction [14]. So far, the most developed application of unfamiliar BP-NGD function concerns the design of RF and microwave phase shifters (PSs) [15]–[24]. The NGD PS was, recently, exploited to develop innovative topologies of antenna array operating with squint-free beamforming [15]–[21]. This type of NGD antenna array application is fundamentally implemented with non-Foster elements using BP-NGD networks [17], [20], [21]. Another type of innovative application was the design of broadband PS using BP-NGD function operating independently to the frequency [22]–[24].

Further innovative work inspired from this BP-NGD PS will be developed in the present paper. But before this point, it would be interesting to investigate more on the unfamiliar NGD function. Recent investigations from research teams [25]–[32] confirm the diversity of BP-NGD topologies. The BP-NGD effect was verified with absorptive filter [25] and interference techniques [26]. A topology of BP-NGD active circuit was implemented by using microwave transversal filter approach [27]. The complexity leads some research works on the design of compact microwave passive circuits [28], [29]. More extensive microwave function aspect as the dual-band BP-NGD behavior was developed in [30]–[33]. The dual-band NGD functions were also implemented with compact circuits [31], [32] and with multi-coupled lines [33].

Despite the progressive state of the art on the BP-NGD circuit design, due to its unfamiliarity, curious questions are still raised by RF and microwave design engineers about the interpretation of the NGD effect. For a deep illustration, an analogy between the filter theory and the NGD function theory was addressed in [34]. Unlike the filter, the NGD function focuses mainly on the negative sign associated to the GD response and not to the magnitude response [34]–[36]. Different types of NGD function

**TABLE 1. State-of-the-art on the different types of NGD circuits.**

References	Type	Passive/Active
[13, 34]	LP-NGD	Active circuit
[35-36]	LP-NGD	Passive circuit
[8-9,14, 20,25-26,28-29]	BP-NGD	Passive circuit
[10-11,13,21,27]	BP-NGD	Active circuit
[36-38]	HP-NGD	Passive circuit
[30-33]	Dual-band BP-NGD	Passive circuit
[39-40]	SB-NGD	Passive circuit

are initiated and identified [35]–[40]. The concept of low-pass (LP) NGD function was proposed in [35]. The BP-NGD [8]–[14], [20]–[29], high-pass (HP) NGD [36]–[38] and stop-band (SB) NGD [39], [40] RF passive circuits transformed from low-pass (LP) NGD cell are introduced.

Table 1 addresses an overview on the state-of-the-art about the existing different types of NGD function which can be implemented either with passive or active circuits. It is important to note the dual-band NGD circuits as proposed in [30]–[33] are completely and ideally different to the type of SB-NGD circuits.

So far most of available research work on the design of NGD circuits can be described as follows:

- The simplest topologies are designed as LP-NGD type function [13], [34]–[36]. For this type, the group delay (GD) is negative from DC to certain higher frequencies.
- The BP-NGD type function containing lower and upper NGD cut-off frequencies are mainly designed for RF and microwave circuits [15]–[34].
- By means of LP- to HP-NGD circuit transform, circuit theory showing few research works was performed are available about the design of HP-NGD function [36]–[38].
- Then, very recent studies revealed the design feasibility of the most innovative types of NGD circuits which are classified as SB-NGD function [39], [40]. And deep investigation can be made for this last type of NGD circuit in order to develop some potential applications.

For this reason, the present paper investigates this SB-NGD function and introduces one of its original application for the design of stair phase microwave circuit. The paper is organized in six sections as follows:

- Section II is focused on the unfamiliar SB-NGD topological description. The theoretical approach permitting the SB-NGD topological identification will be introduced.
- Section III develops the S-matrix model of the identified SB-NGD passive cell. The analytical model in function of the RLC-network parameters constituting the unfamiliar SB-NGD cell will be established. The analytical investigation will be followed by the elaboration of the SB-NGD transfer function (TF) canonical form.

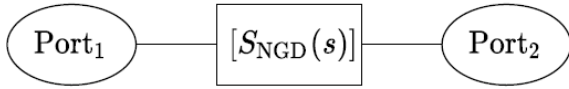


FIGURE 1. Two-port black box of the SB-NGD function.

- In Section IV, the SB-NGD analysis will be developed. Then, the synthesis design equation of circuit in function of the unfamiliar SB-NGD specifications will be formulated.
- Section V is dedicated to the discussion on the unfamiliar SB-NGD function validation results. Comparison between calculated and simulated results of a proof of concept (PoC) will be discussed.
- Section VI is the investigation on the design of stair PS prototype by using the unfamiliar SB-NGD circuit. The design principle of stair PS will be explained. An experimental validation example with a stair unfamiliar PS prototype will be treated.
- Section VII is reserved to the conclusion of the paper.

## II. THEORETICAL INVESTIGATION ON UNFAMILIAR SB-NGD CIRCUIT UNDER CONSIDERATION

This section describes the SB-NGD theory. The main specifications of unfamiliar SB-NGD function are defined. The identification approach of the passive topology based on RLC-lumped circuit will be investigated.

### A. ANALYTICAL DEFINITION OF SB-NGD FUNCTION

Few research work and studies [39], [40] were made so far on the unfamiliar SB-NGD function. Despite the exiting results available in the literature, the existence of this innovative electronic function remains an open question for most of RF and microwave design, fabrication and test engineers. The present paragraph defines analytically the interpretation of the SB-NGD function. We suppose that the two-port black box microwave symmetric and passive system introduced in Fig. 1 is represented analytically by the S-matrix:

$$[S_{NGD}(s)] = \begin{bmatrix} S_{11}(s) & S_{21}(s) \\ S_{21}(s) & S_{11}(s) \end{bmatrix}. \quad (1)$$

with  $s = \omega$  is the Laplace variable expressed in function of angular frequency  $\omega = 2\pi f$ .

We remind that the magnitude of the reflection and transmission coefficients are given by, respectively:

$$S_{11}(\omega) = |S_{11}(j\omega)| \quad (2)$$

$$S_{21}(\omega) = |S_{21}(j\omega)|. \quad (3)$$

To realize the SB-NGD analysis, the following frequency domain responses are essentially needed:

- the phase of the transmission coefficient which is defined by:

$$\varphi(\omega) = \arg[S_{21}(j\omega)] \quad (4)$$

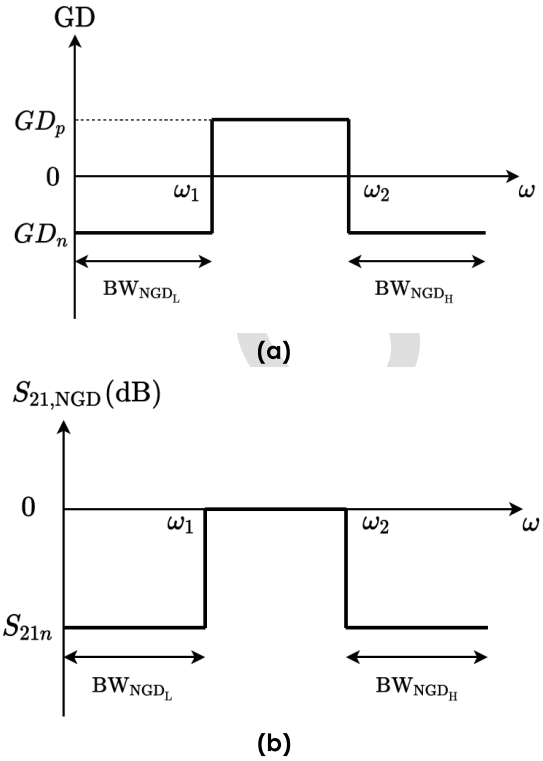


FIGURE 2. (a) GD and (b) transmission coefficient responses of SB-NGD function.

- the frequency dependent GD response which is defined by:

$$GD(\omega) = -\frac{\partial \varphi(\omega)}{\partial \omega}. \quad (5)$$

This system is an NGD function if we can find an angular frequency,  $\omega_x$ , where:

$$GD(\omega_x) < 0. \quad (6)$$

One of specific types associated to NGD function is the SB-NGD concept. The ideal response of SB-NGD function can be represented by Fig. 2(a) by taking:

- The cut-off angular frequencies,  $\omega_1$  and  $\omega_2$ , as roots of equation:

$$GD(\omega) = 0 \Rightarrow GD(\omega_{1,2}) = 0. \quad (7)$$

- The transmission coefficient ideal response is represented in Fig. 2(b) by:

$$S_{21,NGD}(\omega_1 \leq \omega \leq \omega_2) = 1. \quad (8)$$

In Fig. 2(a) and Fig. 2(b):

- the notation  $BW_{NGD_L}$  is used to denote the lower bandwidth,
- and  $BW_{NGD_H}$  for higher bandwidth.

Because of its counterintuitive originality, most of non-specialist electronic and RF/microwave engineers confuse the filter and NGD functions. To avoid the misinterpretation, the

194 following subsection describes the differences between these  
195 two electronic functions.

196 **B. SPECIFIC DIFFERENCES BETWEEN SB FILTER AND**  
197 **SB-NGD FUNCTION**

198 The present analytical illustration is based on the consider-  
199 ation of the frequency dependent parameters associated to  
200 filter and NGD functions:

- 201 • reflection coefficient magnitudes,  $S_{11filter}(f)$  and  $S_{11NGD}(f)$ ,
- 202 • transmission coefficient magnitudes,  $S_{21filter}(f)$  and  $S_{21NGD}(f)$ ,
- 203 • and, GDs  $GD_{filter}(f)$  and  $GD_{NGD}(f)$ .

206 The lower and upper cut-off frequencies in the considered  
207 frequency bands are denoted, respectively:

$$\begin{cases} f_1 = \frac{\omega_1}{2\pi} \\ f_2 = \frac{\omega_2}{2\pi} \end{cases} \quad (9)$$

209 with  $f_1 < f_2$ . Thus, the comparison of the SB-NGD and filter  
210 behaviors and the associated specification can be made within  
211 the frequency band operation bandwidth  $f \in [f_1, f_2]$ . In brief,  
212 the main difference between the classical “stop-band” filter  
213 and the “dual-band” NGD filter are based on which  
214 parameter is used to describe it. The classical filter uses the  
215 magnitude response of the transmission parameter,  $|S_{21}(f)|$ ,  
216 while, for instance, in the “stop-band NGD function”, it is  
217 defined by the NGD frequency band where the group delay  
218 meets the condition  $GD(f) < 0$  [34]. Different parameters  
219 related to the maximum GD of the filter and the maximum  
220 attenuation of NGD must be considered to characterize the  
221 functions.

222 To illustrate the identification of SB NGD topology, a gen-  
223 eral analytical approach will be elaborated in the following  
224 subsection.

225 **C. IDENTIFICATION APPROACH OF SB-NGD TOPOLOGY**

226 The identification approach of SB-NGD topology can be  
227 made by the analogy with the filter [34]. Substantially,  
228 we have identified the SB-NGD passive circuit from the low-  
229 pass (LP) NGD cell based on L-inductance. The elaboration  
230 of SB-NGD cell can be made from the equivalent impedance  
231 given by:

$$Z_a(s) = Ls. \quad (10)$$

233 as the reactive element. As reported in [35] and [36], the  
234 passive cell constituted by an RL-series network mounted in  
235 parallel behaves as a LP-NGD first-order circuit presented in  
236 Fig. 3.

237 We can identify from this LP-NGD cell, the SB-NGD  
238 family by substituting the inductance L by an LC-parallel  
239 network. It yields the two-port circuit represented by the  
240 SB-NGD topology shown in Fig. 4. It acts as a second order  
241 circuit.

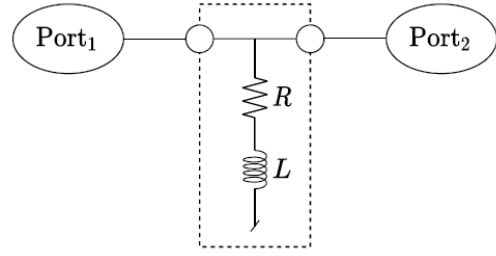


FIGURE 3. LP-NGD cell.

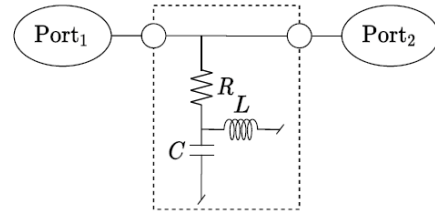


FIGURE 4. SB-NGD cell inspired in the family of the LP-NGD cell shown in Fig. 3.

For this case, the equivalent impedance is given by:

$$Z_b(s) = \frac{Ls}{1 + LCs^2}. \quad (11)$$

To analyze the identified SB-NGD cell, the S-matrix model is elaborated in the following section.

246 **III. S-MATRIX MODEL AND TRANSFER FUNCTION (TF)**  
247 **CANONICAL FORM OF THE SB-NGD TOPOLOGY**

248 Similar to classical RF and microwave circuits, the theo-  
249 retical analysis of the unfamiliar SB-NGD circuit will be  
250 based on the equivalent S-matrix model. Then, the SB-NGD  
251 canonical form will be established before the design equation  
252 formulation.

253 The S-matrix modelling of the SB-NGD topology under  
254 study will be described in the following paragraph.

255 **A. S-MATRIX MODEL OF THE SB-NGD TOPOLOGY**

256 Let us take the terminal reference impedance,  $R_0 = 50 \Omega$ .  
257 We can demonstrate analytically that the impedance matrix  
258 of the SB-NGD topology shown in Fig. 3 is written as:

$$[Z(s)] = \begin{bmatrix} R + Z_b(s) & R + Z_b(s) \\ R + Z_b(s) & R + Z_b(s) \end{bmatrix}. \quad (12)$$

260 According to the circuit and system theory, the associated  
261 S-matrix, introduced in equation (1), can be calculated from  
262 Z-to-S transform:

$$[S_{NGD}(s)] = \left\{ \left( [Z(s)] - \begin{bmatrix} R_0 & 0 \\ 0 & R_0 \end{bmatrix} \right) \times \left( [Z(s)] + \begin{bmatrix} R_0 & 0 \\ 0 & R_0 \end{bmatrix} \right)^{-1} \right\}. \quad (13)$$

Therefore, we establish the reflection and transmission coefficients, respectively, as:

$$S_{11}(s) = S_{22}(s) = \frac{-R_0(1 + LCs^2)}{2R + R_0 + 2Ls + LC(2R + R_0)s^2} \quad (14)$$

$$S_{21}(s) = S_{12}(s) = \frac{2(R + Ls + RLCs^2)}{2R + R_0 + 2Ls + LC(2R + R_0)s^2}. \quad (15)$$

The corresponding SB-NGD analysis is mainly focused on the last expression as described in the next paragraph.

### B. CANONICAL FORM OF SB-NGD TF

The TF associated to the SB-NGD topology is generally represented by the transmission coefficient:

$$T(s) = S_{21}(s). \quad (16)$$

Let us denote the center angular frequency of the positive GD (PGD) as:

$$\omega_0 = 2\pi f_0 \quad (17)$$

where:

$$T(\omega = \omega_0) = |S_{21}(j\omega)|_{\omega=\omega_0} = 1. \quad (18)$$

Then, we denote also the following NGD key parameters, GD value and the transmission coefficient, respectively:

$$\tau_n = GD(\omega_0) \quad (19)$$

$$T_n = |S_{21}(j\omega)|_{\omega=0} = S_{21}(\omega = 0). \quad (20)$$

With the real positive parameter,  $T_n < 1$ , the SB-NGD TF canonical form can be expressed as:

$$T(s) = \frac{T_n(s^2 + \omega_a s + \omega_0^2)}{s^2 + \omega_b s + \omega_0^2} \quad (21)$$

where:

$$\omega_a = \frac{2(1 - T_n)}{T_n \tau_n} \quad (22)$$

$$\omega_b = \frac{2(1 - T_n)}{\tau_n}. \quad (23)$$

By identification with the transmission coefficient expressed in equation (15), we have:

$$T_n = \frac{2R}{2R + R_0} \quad (24)$$

$$\omega_0 = \frac{1}{\sqrt{LC}} \quad (25)$$

$$\tau_n = R_0 C = \frac{R_0}{L\omega_n^2} > 0. \quad (26)$$

In this case, the reflection coefficient proposed in equation (14) can then be rewritten as:

$$S_{11}(s) = \frac{(T_n - 1)(s^2 + \omega_0^2)}{s^2 + \omega_b s + \omega_0^2}. \quad (27)$$

Knowing the S-matrix model, the frequency responses will be analyzed in the following subsection.

### C. ANALYSIS OF S-PARAMETER FREQUENCY RESPONSES

The magnitudes of the reflection and transmission coefficients,  $S_{11}(\omega) = |S_{11}(j\omega)|$  and  $T(\omega) = |T(j\omega)|$  are given, respectively, by:

$$S_{11}(\omega) = \frac{|(1 - T_n)(\omega^2 - \omega_0^2)|}{\sqrt{\tau_n^2(\omega^2 - \omega_0^2)^2 + 4(\omega - T_n\omega_0)^2}} \quad (28)$$

$$T(\omega) = \frac{\sqrt{(T_n\tau_n)^2(\omega^2 - \omega_0^2)^2 + 4(\omega - T_n\omega_0)^2}}{\sqrt{\tau_n^2(\omega^2 - \omega_0^2)^2 + 4(\omega - T_n\omega_0)^2}}. \quad (29)$$

The transmission phase yielded from the transmission coefficient is expressed as:

$$\varphi(\omega) = \varphi_\sigma(\omega) - \varphi_\delta(\omega) \quad (30)$$

with:

$$\varphi_\sigma(\omega) = \arctan \left[ \frac{2(T_n - 1)\omega}{T_n\tau_n(\omega^2 - \omega_0^2)} \right] \quad (31)$$

and:

$$\varphi_\delta(\omega) = \arctan \left[ \frac{2(1 - T_n)\omega}{\tau_n(\omega^2 - \omega_0^2)} \right]. \quad (32)$$

The SB-NGD analysis can be explored from these expressions.

### IV. SB-NGD ANALYSIS AND SYNTHESIS OF THE IDENTIFIED RLC-NETWORK BASED TOPOLOGY

The NGD analysis consists in the identification of the NGD existence condition written in equation (6), in the appropriated frequency bands. The NGD condition can be transformed into a relation between the elements of the topology under study by considering the GD expressed in equation (5). Subsequently, to explore this condition, we need to start with the GD expression versus frequency.

#### A. FREQUENCY DEPENDENT EXPRESSION OF GD

The GD defined in equation (5), which takes into account the transmission phase written in equation (30), is expressed as:

$$GD(\omega) = GD_\delta(\omega) - GD_\sigma(\omega) \quad (33)$$

or

$$GD(\omega) = \frac{\partial \varphi_\delta(\omega)}{\partial \omega} - \frac{\partial \varphi_\sigma(\omega)}{\partial \omega} \quad (34)$$

with

$$GD_\sigma(\omega) = \frac{2\tau_n(1 - T_n)(\omega^2 + \omega_0^2)}{\tau_n^2(\omega^4 + \omega_0^4) + 2[2(1 - T_n)^2 - \tau_n^2\omega_0^2]\omega^2} \quad (35)$$

$$GD_\delta(\omega) = \frac{2\tau_n T_n(T_n - 1)(\omega^2 + \omega_0^2)}{T_n^2\tau_n^2(\omega^4 + \omega_0^4) + 2[2(1 - T_n)^2 - T_n^2\tau_n^2\omega_0^2]\omega^2} \quad (36)$$

The exploration of this GD constitutes the SB-NGD analysis and synthesis to be developed in the next subsection.

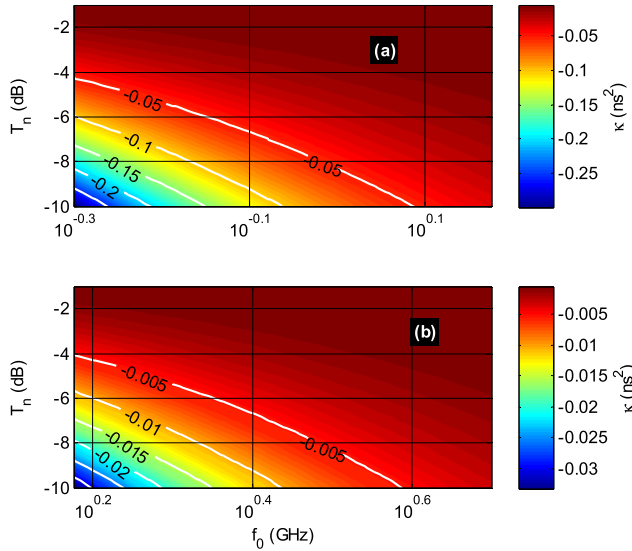


FIGURE 5. Product  $\kappa$  versus  $(f_n, T_n)$  with  $f_n$  (a) from 0.5 to 1.5 GHz and (b) from 1.5 GHz to 5 GHz.

**B. ANALYSIS AT VERY LOW FREQUENCIES ( $\omega \approx 0$ )**

We recall that at very low frequencies,  $\omega \approx 0$ , the reflection and transmission coefficients of equations (28) and (29) become:

$$\begin{cases} S_{11}(\omega = 0) = 1 - T_n \\ S_{21}(\omega = 0) = T_n \end{cases} \quad (37)$$

At the same frequency, the GD introduced in equation (31) is simplified as:

$$GD(\omega \approx 0) = \frac{-2(1 - T_n)^2}{T_n \tau_n \omega_0^2} < 0. \quad (38)$$

For the interpretation of this relation, the mapping of the product:

$$\kappa = GD(f \approx 0) \times GD(f \approx f_0) \quad (39)$$

versus  $(f_0, T_n)$  varied from (0.5 GHz, -10 dB) to (5 GHz, -1 dB) is presented in Figs. 5. It can be seen that the product  $\kappa$  is inversely proportional to  $f_n$  and  $T_n$ . As an interesting remark inferred from the plot of Figs. 5:

- when  $f_n$  increases from 0.5 GHz to 1.5 GHz, the product,  $\kappa$ , decreases from about  $-0.3 \text{ ns}^2$  to  $-299 \text{ ps}^2$ ,
- and when the characteristic frequency varies from 1.5 GHz to 5 GHz, the product,  $\kappa$ , decreases from  $-0.03 \text{ ns}^2$  to  $-26.9 \text{ ps}^2$ .

**C. EXPRESSION OF SB-NGD BANDWIDTH**

We can remark that the GD established in equation (38) is always negative for any values of parameters in the topology proposed in Fig. 4. Moreover, the NGD cut-off frequencies can be determined as the roots of equation (7) by using the GD given in (33). Consequently, we find the cut-off frequencies

given by:

$$\omega_1 = \frac{\sqrt{2(T_n - 1)^2 + T_n(\tau_n \omega_0)^2} + 2\zeta(1 - T_n)}{\tau_n \sqrt{T_n}} \quad (40)$$

$$\omega_2 = \frac{\sqrt{2(T_n - 1)^2 + T_n(\tau_n \omega_0)^2} - 2\zeta(1 - T_n)}{\tau_n \sqrt{T_n}} \quad (41)$$

where:

$$\zeta = \sqrt{(T_n - 1)^2 + T_n(\tau_n \omega_0)^2}. \quad (42)$$

The bandwidth with positive GD (PGD) can be calculated with the relation:

$$BW = \omega_2 - \omega_1. \quad (43)$$

**D. PROPERTIES OF SB-NGD FUNCTION**

Similar to the cases of the most developed types of NGD function as LP-NGD and BP-NGD ones, the SB-NGD function presents some specific analytical properties. It is interesting to note that the cut-off frequencies and PGD center frequency are linked by the equation:

$$\frac{\omega_2 \omega_1}{\omega_0^2} = 1. \quad (44)$$

In addition to this relationship, we remind also that:

- At the central frequency According to equation (18), the magnitude  $T(\omega = \omega_0) = 1$  and the GD at the is equal to  $GD(\omega_0) = \tau_n > 0$ .
- At very low frequency, the magnitude as given in equation (35) must be  $T(\omega \approx 0) < 1$  and the GD at very low frequency  $GD(\omega \approx 0) < 0$ .

In brief, the passive circuit introduced in Fig. 4 enables to have:

$$\begin{cases} GD(\omega < \omega_1) < 0 \\ GD(\omega_1 < \omega < \omega_2) > 0 \\ GD(\omega > \omega_2) < 0 \end{cases} \quad (45)$$

This statement confirms that the circuit introduced in Fig. 4 behaves as a SB-NGD function.

**E. SYNTHESIS AND DESIGN EQUATIONS OF SB-NGD CIRCUIT**

The design of the SB-NGD circuit must start with the specifications of:

- The PGD center frequency,  $\tau_n$ ,
- The attenuation at very low frequency,  $T_n$ ,
- The expected PGD,  $\tau_n$ , which is linked with the NGD at very low frequency,  $\tau_0 = GD_0 < 0$ , given in equation (36).

Therefore, the equations of the SB-NGD circuit  $R$ ,  $L$ , and  $C$  parameters are given by:

$$R = \frac{T_n R_0}{2(1 - T_n)} \quad (46)$$

$$L = \frac{R_0}{\tau_n \omega_0^2} \quad (47)$$



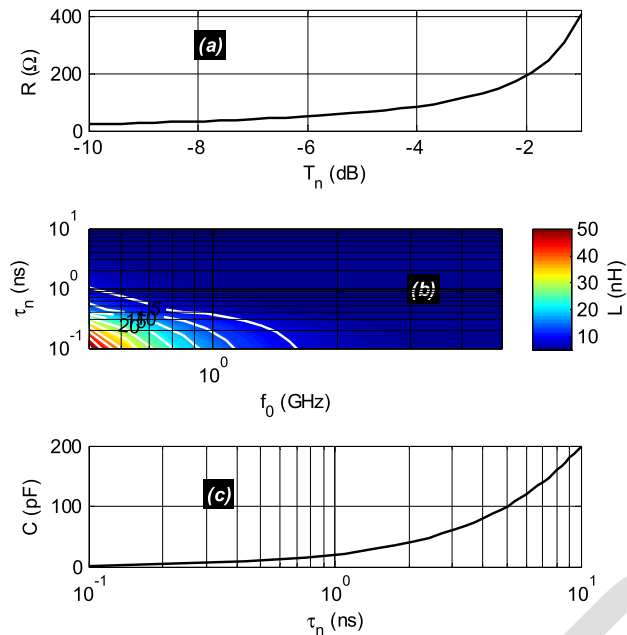


FIGURE 6. Variations of SB-NGD circuit parameters: (a)  $R$ , (b)  $L$ , and (c)  $C$ , versus  $(T_n, \tau_n)$ .

TABLE 2. Minimum and maximum values of synthesized  $R$ ,  $L$  and  $C$  parameters.

Parameters	$T_n$	$\tau_n$	$R$	$L$	$C$
Min.	-10 dB	0.1 ns	23.1 $\Omega$	5.1 pH	2 pF
Max.	-1 dB	10 ns	410 $\Omega$	50.7 nH	0.2 nF

$$C = \frac{\tau_n}{R_0}. \quad (48)$$

We can remind that  $T_n$  must verify the condition,  $0 < T_n < 1$ . The different ranges of  $R$ ,  $L$ , and  $C$  values versus  $(T_n, \tau_n)$  are plotted in Figs. 6. According to these graphical plots, it can be seen that:

- $R$  increases with  $T_n$ ,  $L$  varies inversely proportional to  $T_n$  and  $\tau_n$ , and  $C$  increases proportionally to  $\tau_n$ .
- The  $R$ -variation slope is particularly weak, lower than 10  $\Omega$ /dB, when  $T_n$  is below -6 dB, against the slope above -4 dB, which is more than 100  $\Omega$ /dB.
- The  $C$ -variation presents a slope less than 10 pF/decade when  $\tau_n$  is lower than 1 ns against more than 100 pF/decade when  $\tau_n$  is higher than 1 ns.

Table 2 summarizes the minimal and maximal values of  $R$ ,  $L$ , and  $C$  versus the considered minimal and maximal range of  $(T_n, \tau_n)$ .

To verify the feasibility of the developed SB-NGD theory, PoC practical investigation will be presented in the next section.

## V. VERIFICATION RESULTS WITH PROOF OF CONCEPT (POC) CIRCUIT OF SB-NGD TOPOLOGY

The present section deals with the validations of the SB-NGD topology. After the PoC description, parametric simulations are described in order to quantify the influence of the  $R$ ,

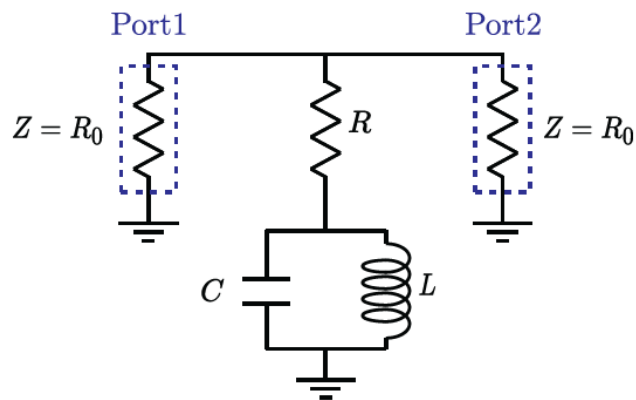


FIGURE 7. Schematic of the simulated SB-NGD circuit PoC.

TABLE 3. Parameters of the SB-NGD circuit PoC.

Description	Parameter	Ideal value
Specifications	Center frequency	$f_0=2.45$ GHz
	BW	$BW_{PGD}=0.3$ GHz
	NGD value	$\tau_n=-0.1$ ns
	Attenuation	$T_0=-3$ dB
Calculated NGD circuit parameters	Resistor	$R=61$ $\Omega$
	Inductor	$L=0.5$ nH
	Capacitor	$C=8.35$ pF

$L$ , and  $C$  component parameters on the NGD behavior. The overall validation aspects are originally focused on analyzing NGD function.

### A. POC DESIGN DESCRIPTION

The SB-NGD circuit design was performed with the application of synthesis equations of  $R$ ,  $L$ , and  $C$  expressed in equations (46), (47), and (48), respectively. Fig. 7 shows the design of the SB-NGD schematic circuit in the environment of the electronic and RF/microwave circuit simulator ADS® from Keysight Technologies. The NGD specifications and designed circuit electrical parameters are indicated in Table 3.

To illustrate the robustness of the SB-NGD behavior, sensitivity analysis with respect to the circuit parameters will be discussed in the following subsection.

### B. SB-NGD RESPONSE SENSITIVITY ANALYSIS

Sensitivity analyses with respect to the resistor,  $R \pm 5\%$ , inductor,  $L \pm 5\%$ , and capacitor,  $C \pm 5\%$ , have been conducted for the robustness of the SB-NGD circuit. The sensitivity analyses enable to explain more explicitly the circuit parameter effects onto the SB-NGD function. The MATLAB® calculations of GD,  $S_{11}$ , and  $S_{21}$  introduced in equation (33), equation (28), and equation (29) to be discussed in the following paragraphs with the S-parameter analytical expressions, are carried out from 2 GHz to 3 GHz.

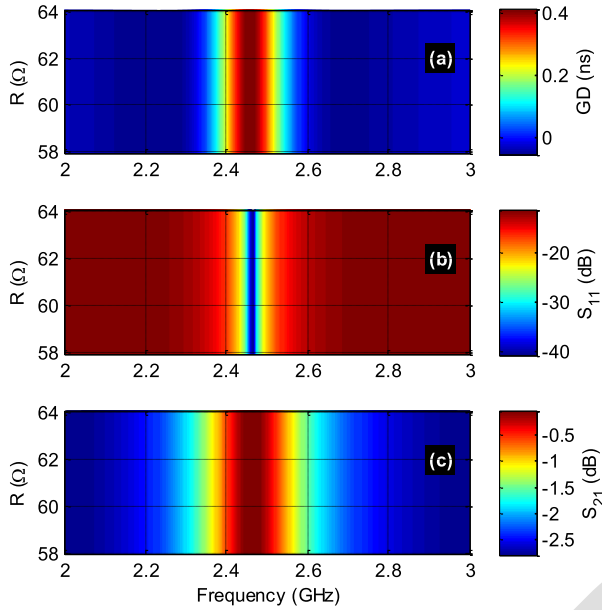


FIGURE 8. Parametric results versus R: (a) GD, (b)  $S_{11}$ , and (c)  $S_{21}$ .

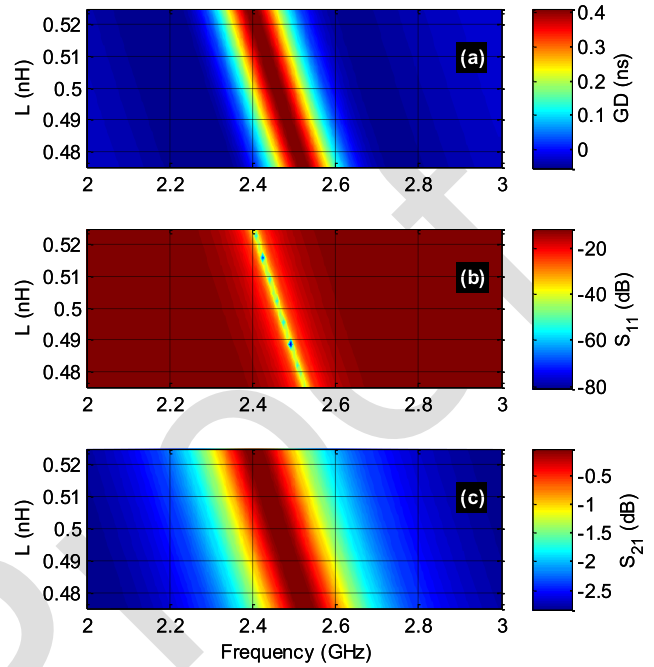


FIGURE 9. Parametric results versus L: (a) GD, (b)  $S_{11}$ , and (c)  $S_{21}$ .

1) SENSITIVITY ANALYSIS VERSUS R

The effect of resistor,  $R$ , was investigated under linear variations from 58  $\Omega$  to 64  $\Omega$  with  $\tau$  fixed values of  $L$  and  $C$ . The calculated results are represented as cartographies with color scale variation of responses in function of couple ( $f_0$ ,  $R$ ). Fig. 8(a), Fig. 8(b), and Fig. 8(c) display the results of the calculations of GD,  $S_{11}$ , and  $S_{21}$ , respectively. The SB-NGD behavior is occurred for all the value of the considered range of  $R$ . It is noteworthy that the specified parameters, center frequency,  $f_0 = 2.458$  GHz,  $GD(f_0) = 0.42$  ns,  $S_{11}(f_0) = -38$  dB, and  $S_{21}(f_0) = -4$  mdB are less sensitive to variation of  $R$ .

2) SENSITIVITY ANALYSIS VERSUS L

The inductor variation effect was investigated via linear sensitivity analysis of inductor  $L$  varied from 4.75 nH to 5.25 nH with fixed resistor and capacitor during the S-parameter calculations. Fig. 9(a), Fig. 9(b), and Fig. 9(c) display the corresponding results.

It can be seen with the three cartographies that the NGD center frequency increases with  $L$ . More rigorous analysis can be done from observation of  $f_0$ ,  $GD(f_0)$ ,  $S_{11}(f_0)$ , and  $S_{21}(f_0)$  variations plotted in Figs. 10(a), Fig. 10(b), and Fig. 10(c), respectively.

3) SENSITIVITY ANALYSIS VERSUS C

This paragraph presents the capacitor variation effect onto the SB-NGD circuit responses.

The analysis is performed with linear sensitivity analysis of capacitor  $C$  varied from 7.93 pF to 8.77 pF with fixed resistor and inductor during the S-parameter calculations. Fig. 11(a), Fig. 11(b), and Fig. 11(c) display the corresponding results. It can be seen with the three cartographies that the NGD

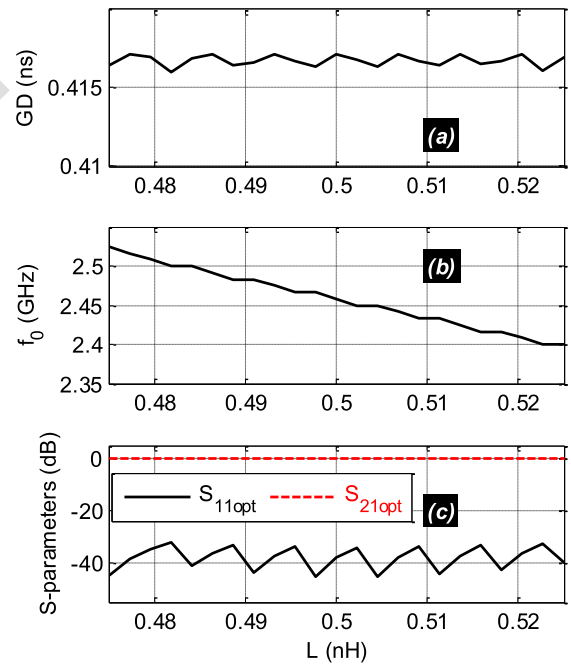


FIGURE 10.  $GD(f_0)$ ,  $f_0$ ,  $S_{11}(f_0)$ , and  $S_{21}(f_0)$  versus L.

center frequency increases with  $C$ . More rigorous observation of  $f_0$  increasing from 2.4 GHz to 2.525 GHz,  $GD(f_0)$ ,  $S_{11}(f_0)$ , and  $S_{21}(f_0)$  variations are plotted in Fig. 12(a), Fig. 12(b), and Fig. 12(c), respectively.

C. DISCUSSION ON CALCULATED AND SIMULATED SB-NGD RESULTS

The PoC of SB-NGD circuit was simulated from 2 GHz to 3 GHz. Comparisons between the calculated (“Calc.”) and simulated (“Simu.”) with ADS® results are displayed in

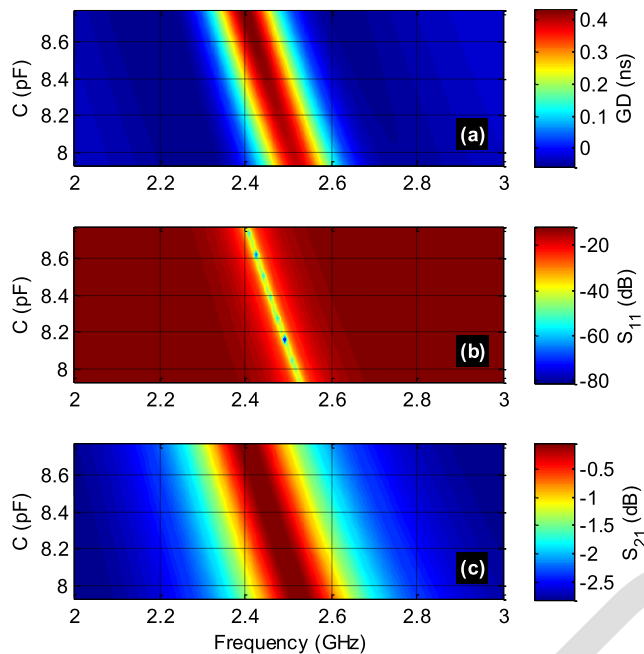


FIGURE 11. Parametric results versus C: (a) GD, (b)  $S_{11}$ , and (c)  $S_{21}$ .

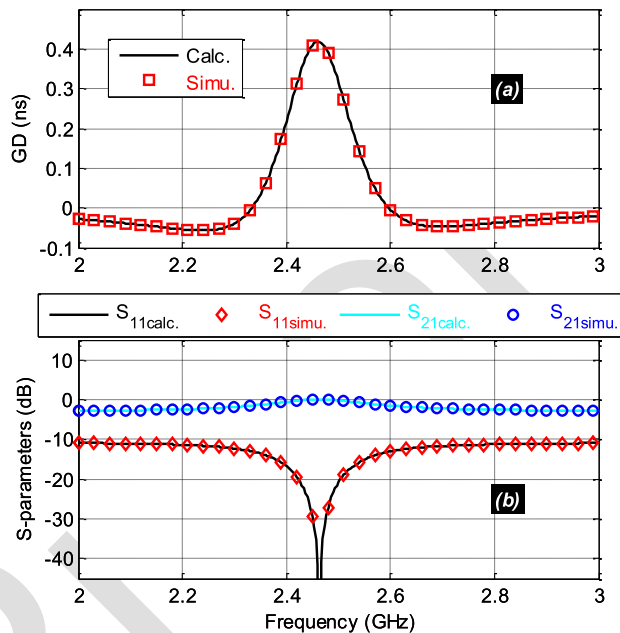


FIGURE 13. Comparisons of calculated and simulated (a) GD and (b) transmission parameters from the SB-NGD PoC shown in Fig. 8.

TABLE 4. Comparison of calculated and simulated SB-NGD prototype parameters.

Approach	$f_0$ (GHz)	$\tau(f_0)$ (ns)	BW (MHz)	$S_{21}(f_0)$ (dB)	$S_{11}(f_0)$ (dB)
Calculated	2.46	4.17	267	-0.42	-17
Simulated	2.46	4.16	268	-0.41	-18

TABLE 5. Comparison of SB NGD circuit specifications with the state-of-the-art.

Approach	$f_0$	$\tau(f_0)$	BW	Attenuation @ $f_0$
[36]	0.5 GHz	2 ns	46 MHz	-0.05 dB
[39]	32 MHz	0.89 ns	83.6 MHz	-7.3 dB
[40]	0.95 kHz	108 $\mu$ s	1.45 kHz	-4.08 dB
This work	2.46 GHz	4.16 ns	268 MHz	-0.41 dB

Table 4 summarizes the differences between the calculated and simulated NGD parameters.

After the SB-NGD sensitivity analysis and feasibility study, an original case of application to design a stair PS for microwave system will be explored in the following section.

#### D. COMPARISON OF SB NGD SPECIFICATIONS

The present subsection proposes a state-of-the-art investigation about the unfamiliar SB NGD function. We can compare the specifications of the considered NGD circuit with the very few research works available in the literature about the SB NGD circuit design [36], [39], [40]. Table 5 summarizes the comparison of NGD at center frequency  $f_0$ , GD  $\tau(f_0)$  at the center frequency, bandwidth BW and also the attenuation at center frequency.

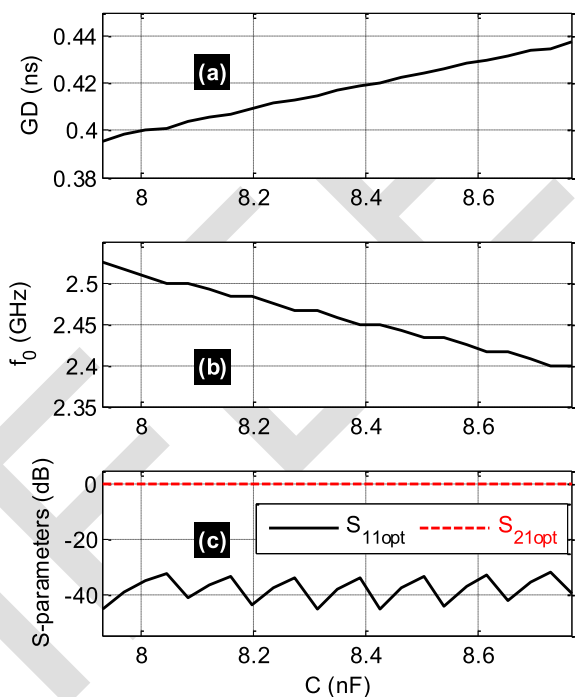


FIGURE 12.  $GD(f_0)$ ,  $f_0$ ,  $S_{11}(f_0)$ , and  $S_{21}(f_0)$  versus C.

Fig. 13. The calculated results were obtained with a program developed in Matlab using S-parameters equations. It can be pointed out that these comparative results present a very good agreement. As expected, and seen in Fig. 13(a), in the working frequency band, the considered circuit PoC presents a SB-NGD behavior around center frequency of approximately  $f_0 = 2.46$  GHz.

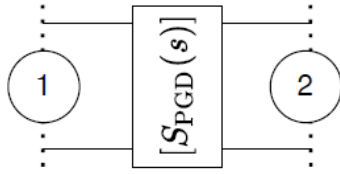


FIGURE 14. Two-port black box of positive group delay (PGD) circuit.

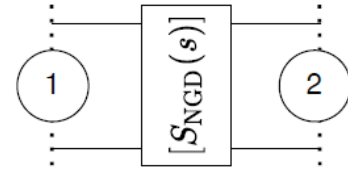


FIGURE 15. Two-port black box of NGD ideal circuit.

512 The present research work is particularly challenging with  
513 the possibility of SB-NGD circuit design operating at higher  
514 central frequency with very low attenuation loss.

515 At this stage, we may wonder about the designability of SB  
516 NGD integrating into a PS. The following section develops  
517 the innovative stair PS design, fabrication and test of the proof  
518 of concept.

#### 519 VI. SB-NGD CIRCUIT BASED-STAIR PS DESIGN, 520 FABRICATION AND TEST

521 As original application of the previously investigated  
522 SB-NGD circuit, we can design an innovative stair PS never  
523 been done before. The next paragraph introduces the principle  
524 of the stair PS.

##### 525 A. THEORETICAL APPROACH OF STAIR PS DESIGNING

526 The present subsection describes the theoretical approach  
527 of SB-NGD function application for stair PS circuit design.  
528 The design is illustrated by graphical diagram representation  
529 based on the S-matrix operation.

##### 530 1) DESIGN PRINCIPLE OF STAIR PS WITH SB-NGD 531 FUNCTION

532 For the basic understanding, we consider the case of two-  
533 step stair PS in the present study. Thus, we assume that the  
534 frequency band of interest is written as:

$$535 \quad BW_L = [\omega_{L1}, \omega_{L2}]. \quad (49)$$

536 The original stair PS under study is ontologically imple-  
537 mented with cascade of ideal PGD and NGD two-port circuits  
538 as introduced in [22]–[24] for the case of BP-NGD circuit.  
539 To illustrate the ideal principle elaborated in the present  
540 subsection, we suppose that the reflection coefficients of the  
541 ideal PGD and NGD two-port circuits are negligible:

$$542 \quad |S_{11,22,PGD}(j\omega)| = |S_{11,22,NGD}(j\omega)| = 0. \quad (50)$$

543 The NGD-function based PS explored in [22]–[24] is speci-  
544 fied by the phase shift value independent to the frequency on  
545 the band of interest. To obtain such a particular behavior, the  
546 PGD and NGD circuits must fulfil certain specific require-  
547 ments as introduced in the following paragraphs.

##### 548 2) IDEAL SPECIFICATION OF PGD BLOCK OF THE NGD-PS 549 CIRCUIT

550 The ideal specification of the PGD block is defined by  
551 the analytical approach by assuming with the constant

(independent of frequency) ideal GD value:

$$552 \quad GD_{PGD}(\omega) = \tau_a > 0. \quad (51) \quad 553$$

554 Figs. 14 represents the S-matrix block of the perfectly access  
555 matched PGD as a two-port circuit which means:

$$556 \quad S_{11,PGD}(j\omega) = S_{22,PGD}(j\omega) \approx 0. \quad (52)$$

557 Therefore, the corresponding S-matrix can be expressed by  
558 the ideal equations:

$$559 \quad [S_{PGD}(j\omega)] = \begin{bmatrix} 0 & S_{21,PGD}(j\omega) \\ S_{21,PGD}(j\omega) & 0 \end{bmatrix} \quad (53)$$

560 knowing that:

$$561 \quad S_{21,PGD}(j\omega) = S_a \exp [j(\varphi_a - \omega\tau_a)] \quad (54)$$

562 with the constant phase,  $\varphi_a$ , and constant magnitude:

$$563 \quad |S_{21,PGD}(j\omega)| = S_a < 1. \quad (55)$$

564 The NGD block must operate in opposite phase of the PGD  
565 one. The NGD block ideal specification will be defined in the  
566 following paragraph.

##### 567 3) IDEAL SPECIFICATION OF NGD BLOCK OF THE NGD-PS 568 CIRCUIT

569 In this case, let us denote the ideal GD value of NGD block  
570 as:

$$571 \quad GD_{NGD}(\omega) = \tau_b < 0. \quad (56)$$

572 The NGD circuit is assumed with constant magnitude:

$$573 \quad |S_{21,NGD}(j\omega)| = S_b < 1 \quad (57)$$

574 and constant phase:

$$575 \quad \arg [S_{21,NGD}(j\omega)] = \varphi_b. \quad (58)$$

576 Figs. 15 represents the S-matrix blocks of the perfectly access  
577 matched NGD system modelled by the ideal equation:

$$578 \quad [S_{NGD}(j\omega)] = \begin{bmatrix} 0 & S_{21,NGD}(j\omega) \\ S_{21,NGD}(j\omega) & 0 \end{bmatrix} \quad (59) \quad 579$$

580 where:

$$581 \quad S_{21,NGD}(j\omega) = S_b \exp [j(\varphi_b - \omega\tau_b)]. \quad (60)$$

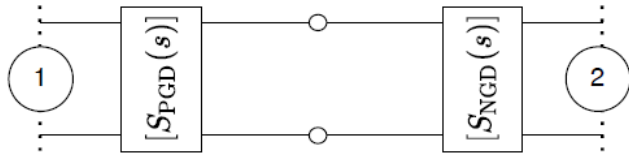


FIGURE 16. Two-port black box of frequency-independent PS constituted by PGD and NGD ideal circuits in cascade.

581 4) IDEAL REPRESENTATION OF STAIR PS WITH SB-NGD  
582 FUNCTION

583 The associated block is illustrated by the diagram of Fig. 16.  
584 Since the reflection coefficients are negligible as defined by  
585 equation (50), it should present the S-matrix product as

$$586 [S_{PS}(j\omega)] = [S_{PGD}(j\omega)] \times [S_{NGD}(j\omega)]. \quad (61)$$

587 By means of 2-D matrices introduced in equation (52) and  
588 equation (59), we have the ideal expression of PS S-matrix  
589 model:

$$590 [S_{PS}(j\omega)] = \begin{bmatrix} 0 & S_{21,PS}(j\omega) \\ S_{21,PS}(j\omega) & 0 \end{bmatrix} \quad (62)$$

591 with

$$592 S_{21,PS}(j\omega) = S_a S_b \exp \{j[\varphi_b + \varphi_b - \omega(\tau_a + \tau_b)]\}. \quad (63)$$

593 In the frequency band of the study, we can realize a frequency  
594 independent PS as illustrated by Fig. 17(a) by choosing the  
595 GD proposed in Fig. 17(b):

$$596 GD_{NGD}(\omega) = -GD_{PGD}(\omega). \quad (64)$$

597 Therefore, it means that we should have:

$$598 \tau_b = -\tau_a. \quad (65)$$

599 The PGD and NGD associated frequency dependent phase  
600 values are given by, respectively:

$$601 \begin{cases} \varphi_{21,PGD}(\omega) = \arg [S_{21,PGD}(j\omega)] = \varphi_{21,PGD}(\omega_{L1}) - \omega\tau_a \\ \varphi_{21,NGD}(\omega) = \arg [S_{21,NGD}(j\omega)] = \varphi_{21,NGD}(\omega_{L1}) - \omega\tau_b \end{cases} \quad (66)$$

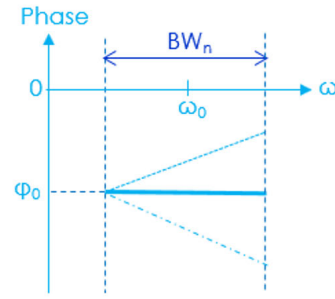
603 5) IDEAL VALUES OF PHASE SHIFT AND GD IN THE EACH  
604 FREQUENCY BAND OF STAIR STEPS

605 The consideration of the dual-band NGD aspect related to  
606 the SB-NGD function as  $BW_L$  and  $BW_H$  shown in Fig. 18(a),  
607 enables to generate a two-step stair PS:

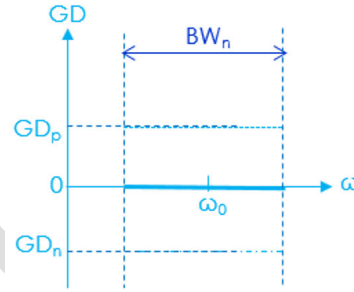
$$608 \begin{cases} \varphi(\omega_{L1} \leq \omega \leq \omega_{L2}) = \varphi_1 \\ \varphi(\omega_{L2} \leq \omega \leq \omega_{H1}) = \varphi_1 - \omega\tau_2 \\ \varphi(\omega_{H1} \leq \omega \leq \omega_{H2}) = \varphi_2 \end{cases} \quad (67)$$

609 with:

$$610 \begin{cases} \varphi_1 = \varphi(\omega_{L1}) = -\omega\tau_1 \\ \varphi_2 = \varphi(\omega_{H1}) = -\omega\tau_3 + \varphi_1 \end{cases} \quad (68)$$

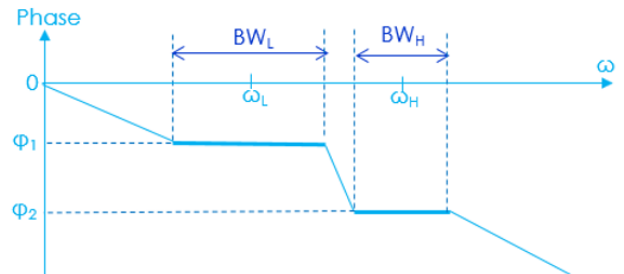


(a)

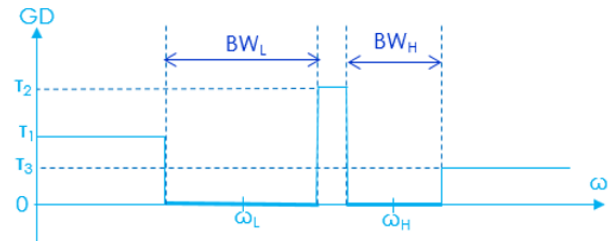


(b)

FIGURE 17. (a) Phase and (b) GD responses of PGD, NGD, and frequency-independent PS.



(a)



(b)

FIGURE 18. (a) Phase and (b) GD ideal responses of two-step stair PS.

In this case, the GD response can be represented as shown in Fig. 18(b), which is defined as:

$$611 \begin{cases} GD(\omega \leq \omega_{x1}) = \tau_1 \\ GD(\omega_{x1} \leq \omega \leq \omega_{x2}) = \tau_2 \\ GD(\omega_{x2} \leq \omega \leq \omega_{y1}) = \tau_3 \\ GD(\omega_{y1} \leq \omega \leq \omega_{y2}) = \tau_2 \end{cases} \quad (69) \quad 613$$

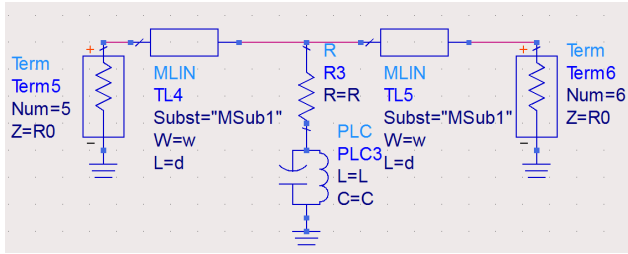


FIGURE 19. Schematic of the designed stair PS prototype.

614 To validate the feasibility of the introduced ideal principle, a  
615 prototype of stair PS circuit PoC will be investigated in the  
616 following subsection.

617 **B. STAIR PS DESIGN AND MODELLING WITH**  
618 **DISTRIBUTED SB-NGD CIRCUIT**

619 The design of the stair PS is explored in the present sub-  
620 section. The design is based on the SB-NGD microstrip dis-  
621 tributed circuit. The equivalent model between lumped and  
622 distributed inductor and capacitor will be proposed.

623 1) DESCRIPTION OF THE DESIGNED PROTOTYPE OF STAIR  
624 PS POC

625 To validate the applicative concept, the developed  
626 SB-NGD function was used to design a stair PS. The pro-  
627 totype of stair PS circuit PoC was designed in hybrid tech-  
628 nology. The PS consists of cascaded PGD constituted by  
629 TL and the SB-NGD circuit. The TL was implemented in  
630 microstrip technology with physical width,  $w$ , and physical  
631 total length,  $d$ . Fig. 19 represents the schematic of the stair  
632 PS PoC designed in the environment of the ADS® elec-  
633 tronic and RF/microwave simulation tools from Keysight  
634 technologies®.

635 First, a “lumped” PS circuit was designed and simulated  
636 with the SB-NGD specified in Table 2. However, the small  
637 values of inductor and capacitor are not available in our labo-  
638 ratory. Therefore, a “distributed” PS circuit was designed  
639 on Isola Astra 3 dielectric substrate with a surface mounted  
640 component (SMC) resistor. The following paragraph will  
641 propose the used distributed model of inductor and capacitor.

642 2) MODEL OF MICROSTRIP DISTRIBUTED INDUCTOR AND  
643 CAPACITOR

644 The distributed microstrip structures, inductance and capac-  
645 itance, widths and lengths are denoted by  $(w_{ind}, d_{ind})$  and  
646  $(w_{cap}, d_{cap})$ , respectively. During the design phase, we have  
647 considered the following constants:

- 648 • the effective permittivity,  $\epsilon_{reff}$ ,
- 649 • the center angular frequency,  $\omega_0 = 2\pi f_0$ ,
- 650 •  $Z_c(w_{ind})$  and  $Z_c(w_{cap})$  are the inductor element charac-  
651 teristic impedances,
- 652 • and  $c$  is the vacuum light speed.

653 According to the TL theory, the lumped inductor component  
654 can be estimated from the distributed physical parameters by

the formula:

$$L = \frac{Z_c(w_{ind}) \tan(\theta_{ind})}{\omega_0} \tag{70}$$

with the electrical angle:

$$\theta_{ind} = \frac{\omega_0 d_{ind} \sqrt{\epsilon_{reff}}}{c} \tag{71}$$

Under the similar approach, the capacitor component can be  
estimated from the formula:

$$C = \frac{\tan(\theta_{cap})}{\omega_0 Z_c(w_{cap})} \tag{72}$$

with:

$$\theta_{cap} = \frac{\omega_0 d_{cap} \sqrt{\epsilon_{reff}}}{c} \tag{73}$$

By choosing the electrical angle respecting the condition,  
we can assume that  $\tan(\theta_{ind}) \approx \theta_{ind}$  and  $\tan(\theta_{cap}) \approx \theta_{cap}$ .  
Consequently, we can estimate the inductor and capacitor  
formulas introduced in equation (70) and equation (72) as:

$$L \approx \frac{Z_c(w_{ind}) d_{ind} \sqrt{\epsilon_{reff}}}{c} \tag{74}$$

$$C \approx \frac{d_{cap} \sqrt{\epsilon_{reff}}}{c Z_c(w_{cap})} \tag{75}$$

After estimation of the distributed components, the designed  
stair PS was fabricated. The results are discussed in the  
following subsection.

673 **C. STAIR PS PROTOTYPING AND EXPERIMENTAL**  
674 **VALIDATION RESULTS**

675 The present subsection is focused on the discussion on  
676 the successfully fabricated two-step stair PS and also the  
677 experimented validation results. Comparisons of results  
678 obtained from calculations, simulation with the ADS® elec-  
679 tronic and RF/microwave simulation tools from Keysight  
680 technologies®, and measurements are discussed.

681 1) DESCRIPTION OF THE FABRICATED PROTOTYPE OF STAIR  
682 PS POC

683 Based on the previously introduced formulas of distributed  
684 self-inductor and capacitor, a prototype of hybrid and  
685 microstrip circuit was designed, fabricated and tested. The  
686 microstrip specifications of substrate susceptible to operate in  
687 the expected frequency band of interest are determined. The  
688 substrate physical characteristics are addressed in Table 6.  
689 The distributed stair PS circuit was implemented.

690 The layout of the stair PS prototype is shown by Fig. 20(a).  
691 The top and bottom view photographs of the fabricated PS  
692 prototype are displayed in Fig. 20(b) and Fig. 20(c). This  
693 stair PS circuit prototype was tested to extract the measured  
694 S-parameter. The following paragraph describes the obtained  
695 results.

**TABLE 6.** Physical parameters of the substrate used in the stair PS circuit.

Structure	Description	Parameters	Values
Substrate	Relative permittivity	$\epsilon_r$	3
	Loss tangent	$\tan(\delta)$	0.0017
	Thickness	$h$	0.76 mm
Metallization conductor	Copper conductivity	$\sigma$	58 MS/s
	Thickness	$t$	35 $\mu\text{m}$
Access line	Length	$d$	2 $\times$ 9 mm
	Width	$w$	1.53 mm
	Propagation delay	$\tau_p$	91.2 ps
SMD component	Resistor	$R$	62 $\Omega$
Distributed inductance structure	Length	$d_{ind}$	5.53 mm
	Width	$w_{ind}$	6.4 mm
Distributed capacitance structure	Length	$d_{cap}$	12 mm
	Width	$w_{cap}$	5 mm

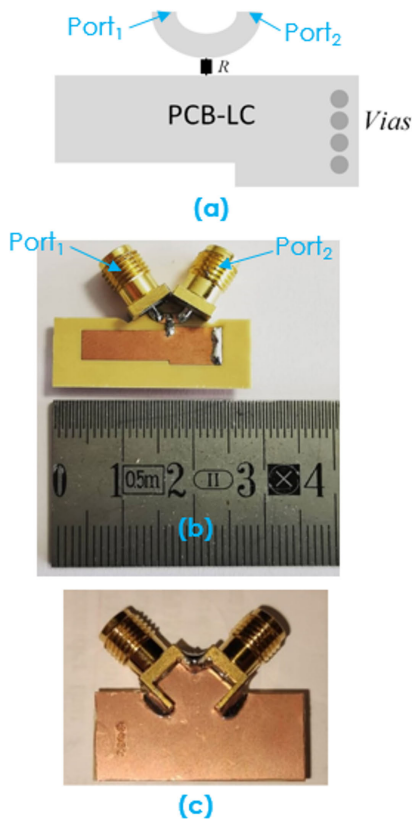


**FIGURE 20.** (a) Layout, (b) top and (c) bottom view photographs of the fabricated stair PS prototype.

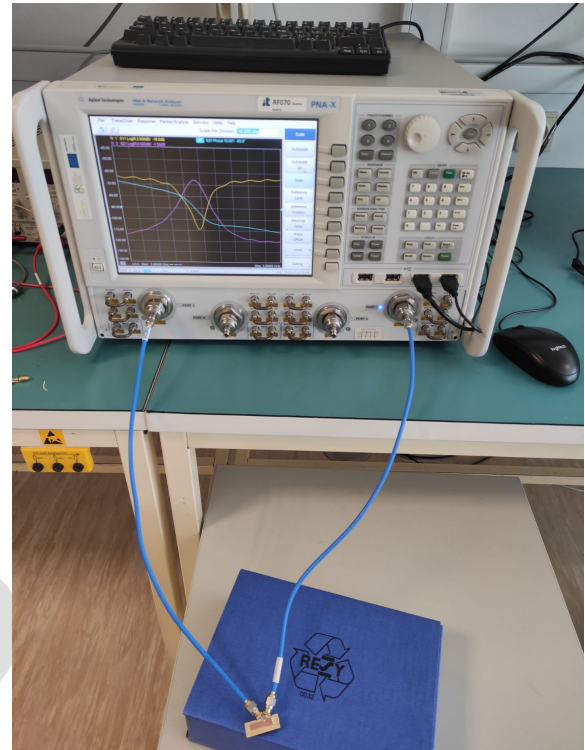


**FIGURE 21.** Configuration of the stair PS SB-NGD prototype experimental setup.

**TABLE 7.** Specifications of the tested two-step stair PS.

Parameters	Lumped		Distributed		Measurement	
	$BW_L$	$BW_H$	$BW_L$	$BW_H$	$BW_L$	$BW_H$
$f_{min}$ (GHz)	2	2.6	2	2.6	2	2.6
$f_{max}$ (GHz)	2.3	3.0	2.3	2.9	2.3	2.9
$\Phi_{mean}$ ( $^\circ$ )	-66	-102	-67.4	-103	-70	-104
$\Delta\Phi$ ( $^\circ$ )	$\pm 2.1$	$\pm 3.2$	$\pm 3$	$\pm 2.4$	$\pm 4$	$\pm 2$
$\Delta S_{21}(f_0)$ (dB)	0.82	1.35	1	1.28	0.88	0.94

10 MHz to 26.5 GHz PNA-X N5242A Network Analyzer from Keysight Technologies®. The experimental setup can be seen in Fig. 21.

During the measurement campaign, the test was made under SOLT calibration. The next paragraph will discuss between the simulated and measured results.

### 3) STAIR PS PROTOTYPE MEASUREMENT VALIDATION

Fig. 22 displays the comparisons between the (lumped and distributed) simulated and measured phase shift and GD results. As expected, they confirm undeniably the two-step stair PS functions. This PoC confirms the feasibility of stair PS. Table 7 summarizes the stair PS specifications.

A good correlation of stair phase values can be underlined with the measured one:

- In the first bandwidth,  $BW_L = 2\text{-}2.3$  GHz, where we have a phase shift of  $-70^\circ \pm 4^\circ$ .
- In the 2nd bandwidth,  $BW_H = 2.6\text{-}3.0$  GHz, the step phase is shifted to  $-104^\circ \pm 2^\circ$ .

## 2) EXPERIMENTAL SETUP CONFIGURATION

As experimental validation, the fabricated stair PS prototype, previously introduced in Fig. 20, was tested in the frequency band from 2 GHz to 3 GHz. Similar to all classical microwave circuits, the stair PS SB-NGD test is based on the S-parameter analysis. The tests were realized with

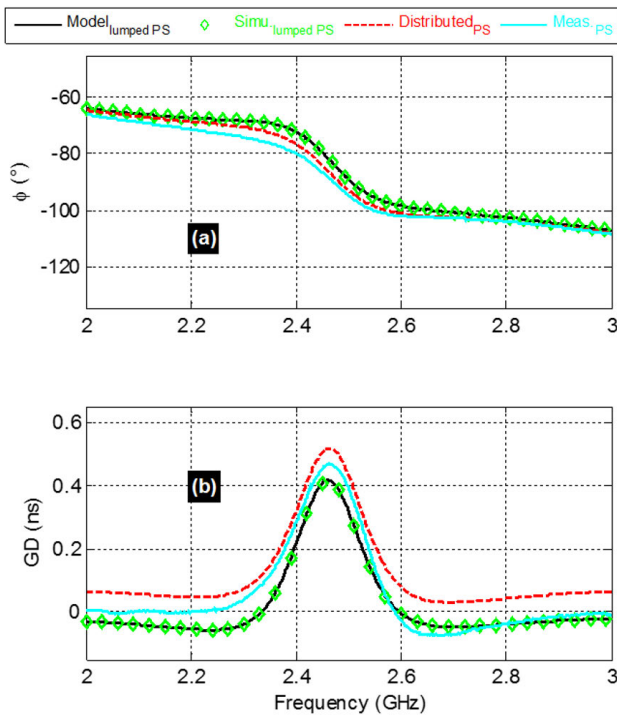


FIGURE 22. Simulated and measured, (a) transmission phase and (b) GD of the stair PS shown in Fig. 20.

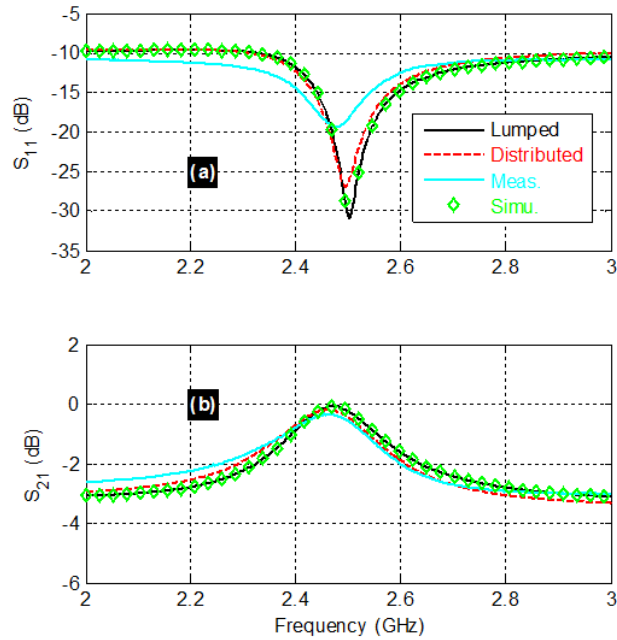


FIGURE 23. Simulated and measured (a)  $S_{11}$  and (b)  $S_{21}$  of the stair PS shown in Fig. 20.

720 Furthermore, the associated reflection and transmission  
 721 coefficients of the stair PS PoC are plotted in Fig. 23. They  
 722 show a good access matching between the two bands ( $BW_L$   
 723 and  $BW_H$ ) and the PS flatness transmission coefficient less  
 724 than 3 dB through the whole range (2-3 GHz).

725  
 726  
 727  
 728  
 729  
 730  
 731  
 732  
 733  
 734  
 735  
 736  
 737  
 738  
 739  
 740  
 741  
 742  
 743  
 744  
 745  
 746

## VII. CONCLUSION

An original theory of SB-NGD circuit is presented. The proposed SB-NGD passive topology was inspired from the LP-NGD cell and the LP-to-SB circuit transform. The S-parameter model is established for the NGD analysis. The different properties of the SB-NGD function are developed.

To confirm the feasibility of the SB-NGD theory, a circuit PoC has been designed and simulated. Sensitivity analyses with respect to the constituting lumped component parameters are performed. It was reported how the SB-NGD response can be sensitivity to the three circuit parameters. An example of SB-NGD circuit application is developed to design a stair PS function with phase shift independent to the frequency. The principle of the stair PS is introduced. Simulations and experimentations illustrate the feasibility of the SB-NGD circuit-based stair PS in two frequency bandwidths.

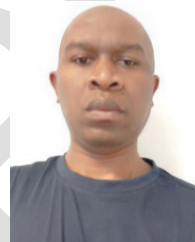
The present research result is a pioneering work about the design of the future communication system. In this optic, the developed stair PS concept can be useful in the future for designing phase array system of innovative multi-beam antenna for the improvement of RF and microwave system control [41].

## REFERENCES

747  
 748 [1] J. Zhang, S. Zhang, Z. Ying, A. S. Morris, and G. F. Pedersen, "Radiation-pattern reconfigurable phased array with p-i-n diodes controlled for 5G mobile terminals," *IEEE Trans. Microw. Theory Techn.*, vol. 68, no. 3, pp. 1103–1117, Mar. 2020.  
 749  
 750 [2] V. Kallnischev, "Analysis of beam-steering and directive characteristics of adaptive antenna arrays for mobile communications," *IEEE Antennas Propag. Mag.*, vol. 43, no. 3, pp. 145–152, Jun. 2001.  
 751  
 752 [3] S.-H. Yan and T.-H. Chu, "A beam-steering and-switching antenna array using a coupled phase-locked loop array," *IEEE Trans. Antennas Propag.*, vol. 57, no. 3, pp. 638–644, Mar. 2009.  
 753  
 754 [4] A. Hakkarainen, J. Werner, K. R. Dandekar, and M. Valkama, "Widely-linear beamforming and RF impairment suppression in massive antenna arrays," *J. Commun. Netw.*, vol. 15, no. 4, pp. 383–397, Aug. 2013.  
 755  
 756 [5] Y. Li, M. F. Iskander, Z. Zhang, and Z. Feng, "A new low cost leaky wave coplanar waveguide continuous transverse stub antenna array using metamaterial-based phase shifters for beam steering," *IEEE Trans. Antennas Propag.*, vol. 61, no. 7, pp. 2619–2625, Jul. 2013.  
 757  
 758 [6] S. S. Oh and L. Shafai, "Compensated circuit with characteristics of lossless double negative materials and its application to array antennas," *IET Microw., Antennas Propag.*, vol. 1, no. 1, pp. 29–38, Feb. 2007.  
 759  
 760 [7] M. A. Antoniadis and G. V. Eleftheriades, "Compact linear lead/lag metamaterial phase shifters for broadband applications," *IEEE Antennas Wireless Propag. Lett.*, vol. 2, pp. 103–106, 2003.  
 761  
 762 [8] G. V. Eleftheriades, O. Siddiqui, and A. K. Iyer, "Transmission line for negative refractive index media and associated implementations without excess resonators," *IEEE Microw. Wireless Compon. Lett.*, vol. 13, no. 2, pp. 51–53, Feb. 2003.  
 763  
 764 [9] O. F. Siddiqui, M. Mojahedi, and G. V. Eleftheriades, "Periodically loaded transmission line with effective negative refractive index and negative group velocity," *IEEE Trans. Antennas Propag.*, vol. 51, no. 10, pp. 2619–2625, Oct. 2003.  
 765  
 766 [10] S. Lucyszyn and I. D. Robertson, "Analog reflection topology building blocks for adaptive microwave signal processing applications," *IEEE Trans. Microw. Theory Techn.*, vol. 43, no. 3, pp. 601–611, Mar. 1995.  
 767  
 768 [11] C. D. Broomfield and J. K. A. Everard, "Broadband negative group delay networks for compensation of oscillators, filters and communication systems," *Electron. Lett.*, vol. 36, no. 23, pp. 1931–1933, Nov. 2000.  
 769  
 770 [12] K.-P. Ahn, R. Ishikawa, and K. Honjo, "Group delay equalized UWB InGaP/GaAs HBT MMIC amplifier using negative group delay circuits," *IEEE Trans. Microw. Theory Techn.*, vol. 57, no. 9, pp. 2139–2147, Sep. 2009.  
 771  
 772  
 773  
 774  
 775  
 776  
 777  
 778  
 779  
 780  
 781  
 782  
 783  
 784  
 785  
 786  
 787  
 788



- [13] B. Ravelo, S. Lalléchére, A. Thakur, A. Saini, and P. Thakur, "Theory and circuit modeling of baseband and modulated signal delay compensations with low- and band-pass NGD effects," *AEU Int. J. Electron. Commun.*, vol. 70, no. 9, pp. 1122–1127, Sep. 2016.
- [14] T. Shao, Z. Wang, S. Fang, H. Liu, and Z. N. Chen, "A full-passband linear-phase band-pass filter equalized with negative group delay circuits," *IEEE Access*, vol. 8, pp. 43336–43343, 2020.
- [15] W. Alomar and A. Mortazawi, "Method of generating negative group delay in phase arrays without using lossy circuits," in *Proc. IEEE Int. Wireless Symp. (IWS)*, Beijing, China, Apr. 2013, pp. 1–4.
- [16] W. Alomar and A. Mortazawi, "Elimination of beam squint in uniformly excited serially fed antenna arrays using negative group delay circuits," in *Proc. IEEE Int. Symp. Antennas Propag.*, Chicago, IL, USA, Jul. 2012, pp. 1–2.
- [17] H. Mirzaei and G. V. Eleftheriades, "Arbitrary-angle squint-free beamforming in series-fed antenna arrays using non-foster elements synthesized by negative-group-delay networks," *IEEE Trans. Antennas Propag.*, vol. 63, no. 5, pp. 1997–2010, May 2015.
- [18] A. Mortazawi and W. Alomar, "Negative group delay circuit," U.S. Patent US20160093958, Mar. 2016.
- [19] M. Zhu and C.-T.-M. Wu, "Reconfigurable series feed network for squint-free antenna beamforming using distributed amplifier-based negative group delay circuit," in *Proc. 49th Eur. Microw. Conf. (EuMC)*, Paris, France, Oct. 2019, pp. 256–259.
- [20] H. Mirzaei and G. V. Eleftheriades, "Realizing non-Foster reactive elements using negative-group-delay networks," *IEEE Trans. Microw. Theory Techn.*, vol. 61, no. 12, pp. 4322–4332, Dec. 2013.
- [21] T. Zhang, R. Xu, and C.-T. M. Wu, "Unconditionally stable non-foster element using active transversal-filter-based negative group delay circuit," *IEEE Microw. Wireless Compon. Lett.*, vol. 27, no. 10, pp. 921–923, Oct. 2017.
- [22] B. Ravelo, M. Le Roy, and A. Perennec, "Application of negative group delay active circuits to the design of broadband and constant phase shifters," *Microw. Opt. Technol. Lett.*, vol. 50, no. 12, Dec. 2008, pp. 3077–3080.
- [23] B. Ravelo, A. Pérennec, and M. L. Roy, "Synthesis of frequency-independent phase shifters using negative group delay active circuit," *Int. J. RF Microw. Comput.-Aided Eng.*, vol. 21, no. 1, pp. 17–24, Jan. 2011.
- [24] B. Ravelo, "Distributed NGD active circuit for RF-microwave communication," *AEU Int. J. Electron. Commun.*, vol. 68, no. 4, pp. 282–290, Apr. 2014.
- [25] L.-F. Qiu, L.-S. Wu, W.-Y. Yin, and J.-F. Mao, "Absorptive bandstop filter with prescribed negative group delay and bandwidth," *IEEE Microw. Wireless Compon. Lett.*, vol. 27, no. 7, pp. 639–641, Jul. 2017.
- [26] Z. Wang, Y. Cao, T. Shao, S. Fang, and Y. Liu, "A negative group delay microwave circuit based on signal interference techniques," *IEEE Microw. Wireless Compon. Lett.*, vol. 28, no. 4, pp. 290–292, Apr. 2018.
- [27] C.-T. M. Wu and T. Itoh, "Maximally flat negative group-delay circuit: A microwave transversal filter approach," *IEEE Trans. Microw. Theory Techn.*, vol. 62, no. 6, pp. 1330–1342, Jun. 2014.
- [28] G. Liu and J. Xu, "Compact transmission-type negative group delay circuit with low attenuation," *Electron. Lett.*, vol. 53, no. 7, pp. 476–478, Mar. 2017.
- [29] T. Shao, Z. Wang, S. Fang, H. Liu, and S. Fu, "A compact transmission line self-matched negative group delay microwave circuit," *IEEE Access*, vol. 5, pp. 22836–22843, 2017.
- [30] H. Choi, Y. Jeong, J. Lim, S.-Y. Eom, and Y.-B. Jung, "A novel design for a dual-band negative group delay circuit," *IEEE Microw. Wireless Compon. Lett.*, vol. 21, no. 1, pp. 19–21, Jan. 2011.
- [31] G. Chaudhary, Y. Jeong, and J. Lim, "Miniaturized dual-band negative group delay circuit using dual-plane defected structures," *IEEE Microw. Wireless Compon. Lett.*, vol. 24, no. 8, pp. 521–523, Aug. 2014.
- [32] T. Shao, S. Fang, Z. Wang, and H. Liu, "A compact dual-band negative group delay microwave circuit," *Radioengineering*, vol. 27, no. 4, pp. 1070–1076, Dec. 2018.
- [33] X. Zhou, B. Li, N. Li, B. Ravelo, X. Hu, Q. Ji, F. Wan, and G. Fontgalland, "Analytical design of dual-band negative group delay circuit with multi-coupled lines," *IEEE Access*, vol. 8, pp. 72749–72756, 2020.
- [34] B. Ravelo, "Similitude between the NGD function and filter gain behaviours," *Int. J. Circuit Theory Appl.*, vol. 42, no. 10, pp. 1016–1032, Oct. 2014.
- [35] B. Ravelo, "First-order low-pass negative group delay passive topology," *Electron. Lett.*, vol. 52, no. 2, pp. 124–126, Jan. 2016.
- [36] B. Ravelo, "On the low-pass, high-pass, bandpass and stop-band NGD RF passive circuits," *URSI Radio Sci. Bull.*, vol. 2017, no. 363, pp. 10–27, Dec. 2017.
- [37] M. Guerin, F. Wan, K. Gorshkov, X. Huang, B. Tishchuk, F. E. Saha, G. Chan, S. Baccar, W. Rahajandraibe, and B. Ravelo, "High-pass NGD characterization of resistive-inductive network based low-frequency circuit," *COMPEL Int. J. Comput. Math. Electr. Electron. Eng.*, vol. 40, no. 5, pp. 1032–1049, Oct. 2021.
- [38] R. Yang, X. Zhou, S. S. Yazdani, E. Sambatra, F. Wan, S. Lalléchére, and B. Ravelo, "Analysis, design and experimentation of high-pass negative group delay lumped circuit," *Circuit World*, pp. 1–25, 2021.
- [39] M. Guerin, Y. Liu, A. Douyere, G. Chan, F. Wan, S. Lallechere, W. Rahajandraibe, and B. Ravelo, "Design and synthesis of inductorless passive cell operating as stop-band negative group delay function," *IEEE Access*, vol. 9, pp. 100141–100153, 2021.
- [40] S. Fenni, F. Haddad, K. Gorshkov, B. Tishchuk, A. Jaomyari, F. Marty, G. Chan, M. Guerin, W. Rahajandraibe, and B. Ravelo, "AC low-frequency characterization of stop-band negative group delay circuit," *Prog. Electromagn. Res. C*, vol. 115, pp. 261–276, 2021.
- [41] H. Liu, S. Gao, and T. H. Loh, "Compact dual-band antenna with electronic beam-steering and beamforming capability," *IEEE Antennas Wireless Propag. Lett.*, vol. 10, pp. 1349–1352, 2011.



**BLAIZE RAVELO** (Member, IEEE) is currently a University Full Professor with NUIST, Nanjing, China. His research interest includes multi-physics and electronics engineering. He is a Lecturer on circuit and system theory, STEM (science, technology, engineering and maths), and applied physics. He is a pioneer of the negative group delay (NGD) concept about  $t < 0$  signal travelling physical space. This extraordinary concept is potentially useful for anticipating and prediction all kind of information. He was the Research Director of 11 Ph.D. students (ten defended), postdocs, research engineers, and master internships. With U.S., Chinese, Indian, European, and African partners, he is actively involved and contributes on several international research projects (ANR, FUI, FP7, INTERREG, H2020, Euripides<sup>2</sup>, Eurostars). He is a member of *Electronics Letters* (IET) Editorial Board as a Circuit and System Subject Editor. He has been a member of the Scientific Technical Committee of Advanced Electromagnetic Symposium (AES), since 2013. He is ranked in Top 2% world's scientists based on years (2020–2021) by Stanford University, USA (<https://elsevier.digitalcommonsdata.com/datasets/btchxktzyw/3>). He has Google Scholar H-index (2021) = 24 and i10-index (2021) = 72. He is a member of the research groups IEEE, URSI, GDR Ondes, and Radio Society, and (co) authors of more than 360 scientific research papers in new technologies published in international conference and journals. He is an IEEE Member since 2007 and regularly invited to review papers submitted for publication to international journals (IEEE TRANSACTIONS ON MICROWAVE THEORY AND TECHNIQUES, IEEE TRANSACTIONS ON CIRCUITS AND SYSTEMS, IEEE TRANSACTIONS ON ELECTROMAGNETIC COMPATIBILITY, IEEE TRANSACTIONS ON INDUSTRIAL ELECTRONICS, IEEE ACCESS, IET CDS, and IET MAP) and books (Wiley and Intech Science).

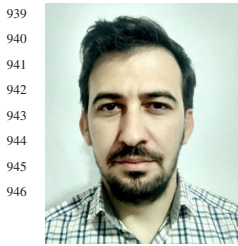


**GLAUCIO FONTGALLAND** (Senior Member, IEEE) was born in Fortaleza, Ceará, Brazil, in March 1966. He was graduated and the M.S. degree in electrical engineering from the Universidade Federal de Campina Grande (UFCG), Campina Grande, Brazil, 1990 and 1993, respectively, and the Ph.D. degree in electronics from the Institut National Polytechnique de Toulouse—ENSEEIH (1999), Toulouse, France, where his thesis work was nominated for the Leopold

Escande Award 1999.

From 2010 to 2012, he was a Visiting Scholar at ElectroScience Laboratory, The Ohio State University (OSU), Columbus, OH, USA. He is currently a Full Professor with the Universidade Federal de Campina Grande (UFCG), Campina Grande, Brazil, where he develops research on: electromagnetic modeling, EMC, EMI, ESD, RFID, UWB, propagation, and antennas for various applications. He has published more than 200 papers in journal and conferences.

932 Prof. Fontgalland is a member of the Sociedade Brasileira de Micro-ondas  
 933 e Optoeletrônica (SBMO), Sociedade Brasileira de Eletromagnetismo  
 934 (SBMag), Sociedade Brasileira de Microeletrônica (SBMicro), and The  
 935 Applied Computational Electromagnetics Society (ACES). He is the past  
 936 IEEE AP-S Chapter Chair and a member of the 2020 IEEE AP-S Student  
 937 Design Contest and 2020 IEEE AP-S Field Awards Evaluation. Since 2019,  
 938 he is an Associate Editor at IEEE LATIN AMERICA TRANSACTIONS.



939 **HUGERLES S. SILVA** (Member, IEEE) received  
 940 the B.Sc., M.Sc., and Ph.D. degrees in electrical  
 941 engineering from UFCG, Brazil, in 2014, 2016,  
 942 and 2019, respectively. He is currently a Postdoc-  
 943 toral Student at the Telecommunications Institute,  
 944 University of Aveiro, Portugal. His main research  
 945 interests include wireless communication, digital  
 946 signal processing, and wireless channel modeling.



947 **JAMEL NEBHEN** (Member, IEEE) received  
 948 the M.Sc. degree in microelectronics from the  
 949 National Engineering School of Sfax, Tunisia,  
 950 in 2007, and the Ph.D. degree in microelectronics  
 951 from Aix-Marseille University, France, in 2012.  
 952 From 2012 to 2018, he worked as a Postdoc-  
 953 toral Researcher at the LIRMM-Lab Montpel-  
 954 lier, IM2NP-Lab Marseille, ISEP Paris, LE2I-Lab  
 955 Dijon, Lab-Sticc Telecom Bretagne Brest, and  
 956 IEMN-Lab Lille, France. Since 2019, he joined

957 the Prince Sattam Bin Abdulaziz University, Al-Kharj, Saudi Arabia, as an  
 958 Assistant Professor. His research interests include the design of anal-  
 959 og and RF integrated circuits, the IoT, biomedical circuit, and sensors  
 960 instrumentation.



961 **WENCESLAS RAHAJANDRAIBE** (Member,  
 962 IEEE) received the B.Sc. degree in electrical  
 963 engineering from the University of Nice Sophia  
 964 Antipolis, France, in 1996, the M.Sc. degree  
 965 (Hons.) in electrical engineering from the Science  
 966 Department, University of Montpellier, France,  
 967 in 1998, and the Ph.D. degree in microelectron-  
 968 ics from the University of Montpellier. In 1998,  
 969 he joined the Montpellier Laboratory of Com-  
 970 puter Science, Robotics, and Microelectronics

971 (LIRMM), Microelectronics Department, University of Montpellier. In 2003,  
 972 he joined the Microelectronic Department, Institute Materials Microelec-  
 973 tronics Nanosciences of Provence (IM2NP), Marseille, France, where he  
 974 was an Associate Professor. Since 2014, he has been a Professor at Aix-  
 975 Marseille University, where he heads the Integrated Circuit Design Group of  
 976 the IM2NP Laboratory. He is currently a Full Professor with Aix-Marseille

977 University. He is regularly involved to participate and to lead national  
 978 and international research projects (ANR, H2020, FP7 KIC-InnoEnergy).  
 979 He directed and co-supervised 18 Ph.D. and 15 master students. His research  
 980 interests involve AMS and RF circuit design from transistor to architectural  
 981 level. His present research activity is focused on ultralow power circuit  
 982 design for smart sensor interface and embedded electronic in bioelectronic  
 983 and e-health applications, wireless systems, design technique, and architec-  
 984 ture for multi-standard transceiver. He is the author or coauthor of more  
 985 than 150 papers published in refereed journals and conferences and holds  
 986 11 patents. He is an Expert of the ANR, the French Agency for Research.  
 987 He has served on program committees of IEEE NEWCAS and ICECS.  
 988 He has been and is a Reviewer of contributions submitted to several IEEE  
 989 conferences and journals, such as ISCAS, NEWCAS, MWSCAS, ESSCIRC,  
 990 ESSDERC, RFIC, IEEE TRANSACTIONS ON CIRCUITS AND SYSTEMS—I, IEEE  
 991 TRANSACTIONS ON CIRCUITS AND SYSTEMS—II, and *Electronics Letters* (IET).



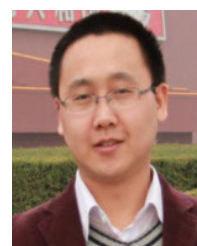
992 **MATHIEU GUERIN** (Member, IEEE) received  
 993 the Engineering degree in microelectronics  
 994 and telecommunications from Polytech Mar-  
 995 seille, in 2010, and the master's degree (by  
 996 Research) in integrated circuits design the Ph.D.  
 997 degree from Aix-Marseille University, in 2010.  
 998 He worked as the Technical Leader of the  
 999 Analog and Radio-Frequency Design Team at  
 1000 IDEMIA-StarChip for five years and designed  
 1001 chips embedded in SIM cards and contactless

1002 bank cards with biometric recognition. In 2020, he joined Aix-Marseille  
 1003 University, as an Assistant Professor, where he joined the CCSI Team of the  
 1004 IM2NP Laboratory. His research interest includes the design and synthesis  
 1005 of circuits in digital electronics. He is also working on methods of modeling  
 1006 and characterizing circuits in analog electronics.



1007 **GEORGE CHAN** (Senior Member, IEEE) received  
 1008 the B.Eng. (Hons.) degree in electronic and com-  
 1009 munication engineering from the City University  
 1010 of Hong Kong and the M.Sc. degree in electronic  
 1011 and information engineering from The Hong Kong  
 1012 Polytechnic University.

1013 He is currently a Senior Product Safety Engi-  
 1014 neer at ASM Pacific Technology Ltd. His research  
 1015 interests include electromagnetic safety, EMC  
 1016 measurement, and EMC management. He has  
 1017 coauthored several technical publications in international journals and con-  
 1018 ference proceedings. He is a member of IEEE EMC Society TC1 on EMC  
 1019 Management. He is also a member of the IEEE International Commit-  
 1020 tee for Electromagnetic safety (ICES) Standards Coordinating Committee  
 1021 (SCC39) and a TC95 Sub-Committee Member. He is an International Elec-  
 1022 trotechnical Commission (IEC) Expert and a Committee Member of IEC  
 1023 TC106/PT63184 on Method for the assessment of electric, magnetic and  
 1024 electromagnetic fields associated with human exposure.



1025 **FAYU WAN** (Member, IEEE) received the Ph.D.  
 1026 degree in electronic engineering from the Uni-  
 1027 versity of Rouen, Rouen, France, in 2011.  
 1028 From 2011 to 2013, he was a Postdoctoral Fellow  
 1029 with the Electromagnetic Compatibility Labora-  
 1030 tory, Missouri University of Science and Tech-  
 1031 nology, Rolla. He is currently a Full Professor  
 1032 with the Nanjing University of Information Sci-  
 1033 ence & Technology, Nanjing, China. His current  
 1034 research interests include negative group delay cir-  
 1035 cuits, electrostatic discharge, electromagnetic compatibility, and advanced  
 1036 RF measurement.